Pressure effects on structures formed by entropically driven self-assembly: Illustration for denaturation of proteins

Takashi Yoshidome,[1] Yuichi Harano,[2] and Masahiro Kinoshita[1,*]
[1]*Institute of Advanced Energy, Kyoto University, Uji, Kyoto 611-0011, Japan*
[2]*Global Edge Institute, Tokyo Institute of Technology, Nagatsuta-cho, Midori-ku, Yokohama 226-8501, Japan*
(Received 16 July 2008; published 20 January 2009)

We propose a general framework of pressure effects on the structures formed by the self-assembly of solute molecules immersed in solvent. The integral equation theory combined with the morphometric approach is employed for a hard-body model system. Our picture is that protein folding and ordered association of proteins are driven by the solvent entropy: At low pressures, the structures almost minimizing the excluded volume (EV) generated for solvent particles are stabilized. Such structures appear to be even more stabilized at high pressures. However, it is experimentally known that the native structure of a protein is unfolded, and ordered aggregates such as amyloid fibrils and actin filaments are dissociated by applying high pressures. This initially puzzling result can also be elucidated in terms of the solvent entropy. A clue to the basic mechanism is in the phenomenon that, when a large hard-sphere solute is immersed in small hard spheres forming the solvent, the small hard spheres are enriched near the solute and this enrichment becomes greater as the pressure increases. We argue that "attraction" is entropically provided between the solute surface and solvent particles, and the attraction becomes higher with rising pressure. Due to this effect, at high pressures, the structures possessing the largest possible solvent-accessible surface area together with sufficiently small EV become more stable in terms of the solvent entropy. To illustrate this concept, we perform an analysis of pressure denaturation of three different proteins. It is shown that only the structures that have the characteristics described above exhibit interesting behavior. They first become more destabilized relative to the native structure as the pressure increases, but beyond a threshold pressure the relative instability begins to decrease and they eventually become more stable than the native structure.

DOI: 10.1103/PhysRevE.79.011912 PACS number(s): 87.15.Zg, 82.60.Lf

I. INTRODUCTION

It has been shown in theoretical calculations that a variety of self-assembling and ordering processes in biological systems, such as protein folding, molecular recognition (lock-key interaction), and amyloid-fibril formation, are driven by the solvent entropy [1–9]. Experimental studies have also shown that in protein folding [10], receptor-ligand binding [11], amyloid-fibril formation [12], association of viruses [13], and formation of actin filaments [14,15] the enthalpic and entropic changes are both positive at ambient temperature and pressure, proving that these processes are entropically driven. When these self-assembling processes occur, the excluded volume (EV) generated by the solute molecule or molecules is greatly reduced. Here, the EV is defined as the volume of the space that the centers of solvent particles cannot enter [16]. The EV decrease provides a corresponding increase in the total volume available to the translational motion of solvent particles in the system, leading to a great gain of solvent entropy. In entropically driven self-assembly such as protein folding and aggregation, the structures almost minimizing the EV for solvent particles are stabilized.

It has been observed in experiments that the denaturation of the native structure (pressure denaturation) [17,18] and the dissolution of amyloid fibrils [19], virus assemblies [13], and actin filaments [20,21] occur at high pressures. Harano and Kinoshita have recently made a statistical-mechanical analysis of pressure denaturation of a protein using three-dimensional integral equation theory [22,23]. The protein is modeled as a set of fused hard spheres immersed in hard spheres forming the solvent. It is demonstrated that the pressure denaturation is also driven by the solvent entropy. At high pressures the solvent entropy becomes higher when the protein takes a specific unfolded structure. The unfolded structure is moderately less compact than the native structure (i.e., the EV is only moderately larger) and characterized by a cleft and/or swelling and solvent penetration into the interior. These characteristics are in good accord with the experimental observations [17,18].

It is, however, difficult to give an interpretation of the result by Harano and Kinoshita in terms of the solvent-entropy effect because it appears that the native structure with almost the smallest EV seems to become more stable as the pressure increases. For example, within the framework of the Asakura-Oosawa (AO) theory [24,25], which is widely used as a simple way of understanding the EV effect, the entropic gain upon self-assembly is given by $-k_B N_S \Delta V_{ex}/V = -k_B \rho_S \Delta V_{ex}$ where k_B is the Boltzmann constant, N_S the total number of solvent molecules in the system, V the system volume, ΔV_{ex} (<0) the decrease in the EV, and $\rho_S = N_S/V$. Since ρ_S becomes higher as the pressure increases, the structures formed by self-assembly should further be stabilized by applying high pressures. This statement clearly conflicts with the theoretical result by Harano and Kinoshita [22,23] as well as the experimental observations [17,18].

In the present paper, we elucidate the microscopic mechanism of pressure effects on the structures formed by the self-

*kinoshit@iae.kyoto-u.ac.jp

assembly driven by the solvent entropy, from a fairly general viewpoint. The integral equation theory is combined with the recently developed morphometric approach [6,26] and applied to a hard-body model system in which all the allowed configurations share the same energy and the system behavior is purely entropic in origin. We argue that the investigation of the solvation entropy (SE) of a large hard-sphere solute inserted into a hard-sphere solvent and the solvent density profile near the solute provide important clues to the mechanism of the pressure effects. "Attraction" is entropically provided between the solute surface and solvent particles, and it becomes higher with rising pressure. At low pressures, the structural stability can be argued in terms of the EV. As the pressure increases, however, the requirement that the solvent-accessible surface area (ASA) be the largest becomes progressively more imperative due to the strong attraction. (Here, the ASA is the area of the surface that is accessible to centers of solvent particles [16].) Upon the pressure-induced structural transition, the ASA increase must be as large as possible while the EV increase must be kept sufficiently small. The structures satisfying these requirements are stabilized at high pressures.

As an illustration of the present picture, we perform an analysis of pressure denaturation of three representative proteins. Several structures are considered for each protein and their relative stability is calculated. Most of the structures are increasingly more destabilized than the native structure with rising pressure. However, a certain class of structures exhibits different behavior. As the pressure increases, they first become more destabilized relative to the native structure, but beyond a threshold pressure the relative instability begins to decrease rather rapidly and they eventually become more stable than the native structure. They are characterized by only a moderate increment of the EV and considerably larger ASA, which is in good accord with the experimental results known for pressure denaturation of proteins. We also discuss the dissolution of amyloid fibrils caused at high pressures and argue that it can be understood within the same theoretical framework.

II. MODEL AND THEORY

A. Integral equation theory

Hard-sphere solutes of diameter d_U are immersed in hard spheres of diameter d_S forming the solvent. All the solute and solvent particles interact through the hard-sphere potential. As described above, the analysis of this simple, reference system using integral equation theory provides an important clue to the mechanism of pressure effects on the structures formed by the entropically driven self-assembly. The subscripts "S" and "U" represent "solvent" and "solute," respectively. The Ornstein-Zernike (OZ) equation for the mixture can be written as

$$\eta_{\alpha\beta}(r) = \sum_{\gamma} \rho_{\gamma} \int c_{\alpha\gamma}(|\mathbf{r}-\mathbf{r}'|)[\eta_{\gamma\beta}(r') + c_{\gamma\beta}(r')]d\mathbf{r}', \tag{1a}$$

$$\eta_{\alpha\beta}(r) = h_{\alpha\beta}(r) - c_{\alpha\beta}(r), \quad \alpha,\beta = \mathrm{S},\mathrm{U}, \tag{1b}$$

where h and c are the total and direct correlation functions, respectively, $d\mathbf{r}'$ represents spatial integration, and ρ is the number density. The closure equation is expressed by [27]

$$h_{\alpha\beta}(r) + 1 = \exp[-u_{\alpha\beta}(r)/(k_B T) + h_{\alpha\beta}(r) - c_{\alpha\beta}(r) + b_{\alpha\beta}(r)], \tag{2}$$

where u is the pair potential, $k_B T$ is the Boltzmann constant times the absolute temperature, and b is the bridge function.

We assume that the solutes are immersed in solvent at infinite dilution ($\rho_U = 0$). The calculation process can then be split into two steps [28–30]:

Step (i). Solve Eqs. (1) and (2) for bulk solvent. Calculate the correlation functions X_{SS} ($X = h, c$).

Step (ii). Solve Eqs. (1) and (2) for the solute-solvent system using the correlation functions obtained in step (i) as input data. Calculate the correlation functions X_{US} ($X = h, c$).

In the present analysis, the hypernetted-chain (HNC) approximation is employed ($b = 0$) because it enables us to calculate the hydration free energy through the simple formula derived by Morita and Hiroike [31,32]:

$$\mu/(k_B T) = 4\pi\rho_S \int \left(\frac{1}{2}\{h_{US}(r)\}^2 - \frac{1}{2} h_{US}(r) c_{US}(r) - c_{US}(r) \right) r^2 dr. \tag{3}$$

The Percus-Yevick (PY) closure gives a pathological density profile of solvent particles which becomes negative near a large solute. The PY closure gives good results only for a hard-sphere mixture with very low size asymmetry. In the present hard-sphere model, μ is equal to $-TS$ where S is the solvation entropy (SE). The solute-solvent pair correlation function $g_{US}(r)$, which represents the reduced density profile of the solvent near the solute, is obtained from

$$g_{US}(r) = h_{US}(r) + 1. \tag{4}$$

As explained in Sec. III B, we discuss two components of the SE: the SE at the solute-solvent pair correlation level and that at the solute-solvent-solvent triplet and higher-order correlation levels. Here we describe the procedure for decomposing the SE into the two components. The SE can be expressed as an expansion in terms of multiparticle correlation functions for a solute immersed in solvent [33]. It comprises components at the solute-solvent pair, solute-solvent-solvent triplet, and higher-order correlation levels. The components representing the solvent-solvent pair, solvent-solvent-solvent triplet, and higher-order correlations perturbed by the solute insertion are also included. The component of the SE at the solute-solvent pair correlation level S^{pair} is given by [33–35]

$$S^{\text{pair}}/k_B = 4\pi\rho_S\left(\int_0^\infty [g_{US}(r)-1]r^2dr - \int_0^\infty g_{US}(r)\ln[g_{US}(r)]r^2dr\right). \quad (5)$$

The first term in the right-hand of Eq. (5) can further be decomposed into the following two terms:

$$4\pi\rho_S\int_0^\infty [g_{US}(r)-1]r^2dr = 4\pi\rho_S\int_{d_{US}}^\infty [g_{US}(r)-1]r^2dr - \frac{4\pi\rho_S d_{US}^3}{3}, \quad (6)$$

where $d_{US}=(d_U+d_S)/2$ and d_U is the solute diameter. The second term in the right-hand side of Eq. (6) represents the contribution from the EV:

$$S_V^{\text{pair}}/k_B = -\frac{4\pi\rho_S d_{US}^3}{3}. \quad (7)$$

We define S_A^{pair} as $S^{\text{pair}}-S_V^{\text{pair}}$:

$$S_A^{\text{pair}}/k_B = 4\pi\rho_S\left(\int_{d_{US}}^\infty [g_{US}(r)-1]r^2dr - \int_{d_{US}}^\infty g_{US}(r)\ln[g_{US}(r)]r^2dr\right). \quad (8)$$

Here the lower limit of the integral of the second term is replaced by d_{US} because $g_{US}(r)=0$ when $r<d_{US}$. S_A^{pair} represents the solvent-entropy change arising from formation of the solute-induced layer of solvent particles. In the SE calculated by the integral equation theory, the solute-solvent-solvent triplet and higher-order correlation terms are also included through the OZ equation, which is formally exact. Therefore,

$$S^{\text{multi}}/k_B = S/k_B - S^{\text{pair}}/k_B \quad (9)$$

represents the SE at the solute-solvent-solvent triplet and higher-order correlation levels. We discuss the physical meaning of S^{multi}/k_B in the Appendix. It should be noted that the solute-solvent-solvent triplet and higher-order correlations are taken into account through the convolution integrals of the solute-solvent and solvent-solvent total correlation functions. For example, the triplet correlation is not expressed in terms of $g(\mathbf{r}_1,\mathbf{r}_2,\mathbf{r}_3)$ but calculated from the convolution integral of the total correlation functions.

For the numerical solution of Eqs. (1) and (2), a sufficiently long range r_L is divided into N grid points ($r_i=i\delta r$, $i=0,1,\ldots,N-1$; $\delta r=r_L/N$) and all of the pair potentials and correlation functions are represented by their values on these points. The basic equations are then rearranged in discrete forms and the large set of nonlinear simultaneous equations is solved using the robust, highly efficient algorithm developed by Kinoshita and co-workers [28–30]. The grid width and the number of grid points are set at $\delta r=0.01d_S$ and $N=8192$, respectively.

B. Models of protein and solvent

The solvation properties of a protein can be analyzed using those of a spherical solute through the morphometric approach explained in the next section. To focus our analysis on the entropic effect, the solvent particles are modeled as hard spheres with diameter $d_S=0.28$ nm, which is the size of water molecules, and a protein is modeled as a set of fused hard spheres. The polyatomic structure, which is crucially important, is accounted for on the atomic level. The diameter of each atom in the protein is set at the σ value of the Lennard-Jones potential parameters of AMBER99. The proteins we examine here are protein G [Protein Data Bank (PDB) code 2GB1], 434 Cro protein (2cro), and the C-terminal domain of ribosomal protein (1ctf).

For each protein, we consider the native structure and unfolded structures. The latter consist of a random-coil state and two rather compact structures referred to as "nonnative 1" and "nonnative 2," respectively. The native structure is taken from the PDB for protein G and from the four-state reduced decoy set [36] for 2cro and 1ctf. We generate 32 random coils for protein G and ten random coils for 2cro and 1ctf. The method of generating the random coils is described in our earlier publication [37]. Nonnative 1 and nonnative 2 are chosen from those treated in our recent studies [38] for protein G. (The nonnative 1 structure and nonnative 2 structure correspond to the compact structure and the swelling structure in [38], respectively. The latter structure is the pressure-denatured structure [22,23,38].) We calculate the SE for all the structures of 2cro and 1ctf in the four-state reduced decoy set at low and high pressures. As shown in Sec. III D, it is found that several structures (class 2) become more stable than the native structure at high pressures while the others (class 1) exhibit increasing relative instability. Nonnative 2 and nonnative 1 are representative structures chosen from class 2 and class 1, respectively. All of the structures are slightly modified to eliminate the unrealistic overlaps of the protein atoms using the standard energy-minimization technique [8].

C. Morphometric approach to solvation entropy and its components

In the morphometric approach [6,26], any of the solvation thermodynamic quantities is expressed using only four geometric measures of a solute with a fixed structure and corresponding coefficients [39]. The resultant morphometric form for the solvation thermodynamic quantity Z is given by

$$Z = C_1V_{ex} + C_2A + C_3X + C_4Y. \quad (10)$$

Here, V_{ex} is the EV, A is the ASA, and X and Y are the integrated mean and Gaussian curvatures of the accessible surface, respectively, and they form the four geometric measures.

The idea of the morphometric form expressed by Eq. (10) is that it separates the geometric properties of the solute molecule and the four coefficients. This separation allows us to determine the four coefficients in simple geometries. They are determined from calculations of Z for the reference system, spherical solutes with various diameters. The morpho-

metric form applied to spherical solutes reduces to

$$Z = C_1\left(\frac{4\pi}{3}d_{\mathrm{US}}^3\right) + C_2(4\pi d_{\mathrm{US}}^2) + 4\pi C_3 d_{\mathrm{US}} + 4\pi C_4. \tag{11}$$

The four coefficients are determined using least squares fitting to Eq. (11). As Z we consider the solvation entropy $-S/k_{\mathrm{B}}$, the SE at the solute-solvent pair correlation level, $-S_{\mathrm{A}}^{\mathrm{pair}}/k_{\mathrm{B}}$, and the SE at the solute-solvent-solvent triplet and higher-order correlation levels, $-S_{\mathrm{A}}^{\mathrm{multi}}/k_{\mathrm{B}}$. We discuss these quantities by multiplying by -1 since the SE contributes to the solvation free energy as $-TS$. It is physically insightful to examine the four coefficients for these quantities. Hereafter, the coefficients in the morphometric form for $-S_{\mathrm{A}}^{\mathrm{pair}}/k_{\mathrm{B}}$ and for $-S^{\mathrm{multi}}/k_{\mathrm{B}}$ are denoted by the superscripts "pair" and "multi," respectively, and those for $-S/k_{\mathrm{B}}$ are written without superscripts. We note that $C_1^{\mathrm{pair}}=\rho_{\mathrm{S}}$ because the EV-dependent term is separated.

Once the four coefficients are determined, Z of a protein with any structure can be obtained by calculating only the four geometric measures. We calculate the four geometric measures by means of Connolly's algorithm [42,43]. Contributions to X and Y from the lines of intersecting spheres and those to Y from the points where three lines meet are also included in the calculation [6]. The high accuracy of the morphometric approach to the SE of a protein has been demonstrated for the hard-sphere solvent [6]. The deviation of the SE by the morphometric approach from that obtained by the three-dimensional (3D) integral equation theory [1,44,45] is less than $\pm 0.7\%$ [6]. We have also confirmed that $-S_{\mathrm{A}}^{\mathrm{pair}}/k_{\mathrm{B}}$ calculated by the morphometric approach is in accordance with that from the 3D integral equation theory [1,44,45]. For example, $-S_{\mathrm{A}}^{\mathrm{pair}}/k_{\mathrm{B}}$ of the native structure of protein G at $\rho_{\mathrm{S}}d_{\mathrm{S}}^3=0.7$ is 132 from the morphometric approach and 148 from the 3D integral equation theory.

III. RESULTS AND DISCUSSION

A. Density profile of solvent near a hard-sphere solute

We first discuss the behavior of the reference system. Figure 1 shows the reduced density profiles of the solvent near a hard-sphere solute of diameter $5d_{\mathrm{S}}$ for several solvent densities in the bulk. The solvent density is a measure of the system pressure. The most striking feature is that a layer within which solvent particles are enriched is formed near the solute, despite the fact that there are no direct attractive interactions between the solute and solvent particles, and the enrichment becomes greater as the pressure increases. Thus, some of the solvent particles in the system are in contact with the solute surface. The contact is important for interpreting the coefficient in morphometric form for solvation entropy in Sec. III B.

B. Pressure effects on the first and second coefficients in morphometric form for solvation entropy and its components

Figure 2(a) shows the density dependence (corresponding to the pressure dependence) of the first and second coefficients C_1 and C_2 in the morphometric form applied to the SE $-S/k_{\mathrm{B}}$. [We do not discuss C_3 and C_4 here because in Eq. (9) C_3X+C_4Y is much smaller than $C_1V_{\mathrm{ex}}+C_2A$.] It is found that $C_1>0$ and $C_2<0$ at any density and that $|C_1|$ and $|C_2|$ become remarkably larger as the density is raised. C_1 and $|C_2|$ increase remarkably with rising pressure, but the increase in the latter is larger: $|C_2|$ is much smaller than C_1 at low pressures, but they are comparable in magnitude at high pressures.

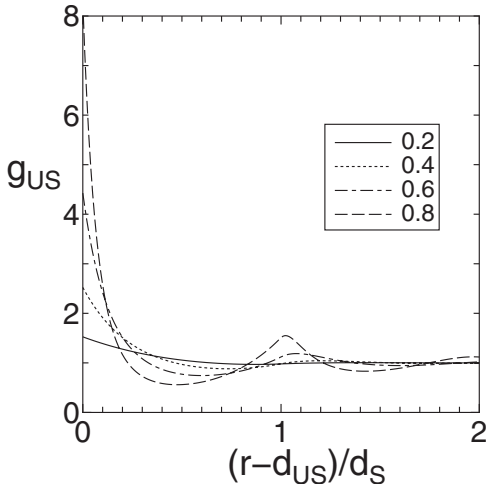

FIG. 1. Reduced density profiles of solvent near a large hard-sphere solute at four different bulk solvent densities, $\rho_{\mathrm{S}}d_{\mathrm{S}}^3=0.2$, 0.4, 0.6, and 0.8.

The positive value of C_1 arises from the solvent-entropy loss caused by the solute insertion. The negative value of C_2 can be interpreted as follows. We first note that the presence

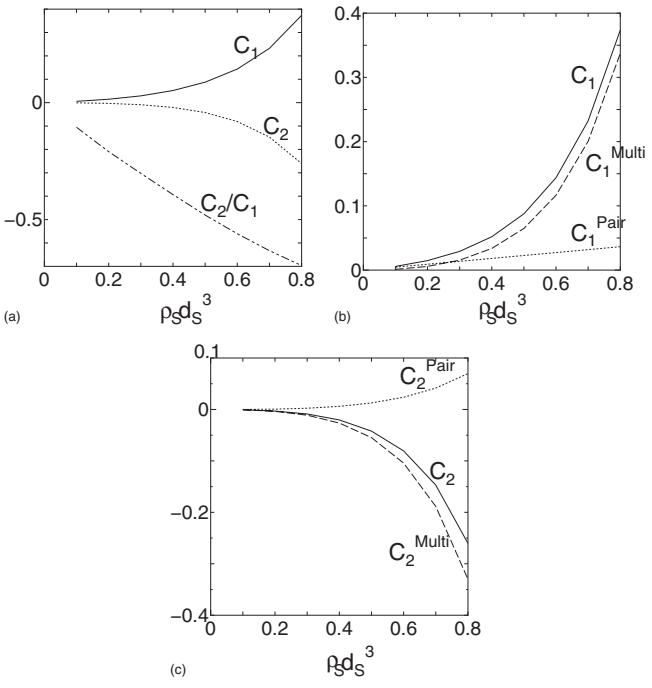

FIG. 2. (a) C_1 ($\mathrm{\AA}^{-3}$), C_2 ($\mathrm{\AA}^{-2}$), C_2/C_1 (Å), (b) C_1 ($\mathrm{\AA}^{-3}$), C_1^{pair} ($\mathrm{\AA}^{-3}$), C_1^{multi} ($\mathrm{\AA}^{-3}$), (c) C_2 ($\mathrm{\AA}^{-2}$), C_2^{pair} ($\mathrm{\AA}^{-2}$), and C_2^{multi} ($\mathrm{\AA}^{-2}$) plotted against solvent density corresponding to the pressure P.

of a solvent molecule generates an EV for the other solvent molecules in the system [22,23]. Due to this solvent crowding, some of the solvent particles are driven to contact the solute surface (note that the contact is observed in Fig. 1). The contact brings the overlap of the EVs generated by the solute and the solvent particles in contact with the solute. As a consequence, the total volume available to the translational motion of the other solvent particles (i.e., the solvent particles well outside the enriched layer in the vicinity of the solute) increases, leading to an entropic gain. The solvent-density profile near the solute is determined by the balance of this entropic gain and the entropic loss for solvent particles in contact with the solute surface. The solvent crowding becomes more serious as the pressure increases, and the entropic attraction between the solute surface and solvent particles becomes stronger and the solvent enrichment near the solute becomes greater.

To show the validity of the picture described in the last paragraph quantitatively, we decompose S into two parts: S^{pair} and S^{multi}. The contribution from the solvent particles in contact with the solute surface is included mostly in S^{pair} because the contact is represented by $g_{\text{US}}(r)$ (see the Appendix). The contact leads to reduction in the crowding of the particles sufficiently far from the solute, and this effect is attributed to the solute-solvent-solvent triplet and higher-order correlations. Thus, the entropic gain is expected to be induced by S^{multi}. The coefficients C_1 and C_2 for S^{pair} and S^{multi} are shown in Figs. 2(b) and 2(c). C_1^{pair} and C_1^{multi} are both positive. On the other hand, C_2^{multi} is negative while C_2^{pair} is positive as shown in Fig. 2(c). The positive value of C_2^{pair} is indicative that the formation of the denser layer of solvent particles near the solute surface gives rise to an entropic loss. It is obvious that $C_2<0$ originates from $C_2^{\text{multi}}<0$. Thus, we can conclude quantitatively that the entropic gain can be ascribed to the reduction in the crowding of the particles sufficiently far from the solute.

C. General framework of pressure effects on structures formed by self-assembly

We consider the solvation entropies of the two structures formed by the self-assembly of a solute molecule or solute molecules at low and high pressures, respectively. Since in Eq. (10) C_3X+C_4Y is much smaller than $C_1V_{\text{ex}}+C_2A$, the difference between the two quantities is approximately given by

$$-S^{\text{high}}/k_{\text{B}}-\{-S^{\text{low}}/k_{\text{B}}\}\simeq C_1(V_{\text{ex}}^{\text{high}}-V_{\text{ex}}^{\text{low}})+C_2(A^{\text{high}}-A^{\text{low}}), \tag{12}$$

where the superscripts "high" and "low" denote the structures stabilized at high and low pressures, respectively. For the pressure denaturation of a protein, for example, "high" and "low" denote the unfolded structure and the native structure, respectively. At high pressures, the structure formed by self-assembly is usually destroyed: The protein is unfolded and the amyloid fibrils are dissolved. The difference $-S^{\text{high}}/k_{\text{B}}-\{-S^{\text{low}}/k_{\text{B}}\}$ represents the negative of the solvent-entropy change upon destruction. $V_{\text{ex}}^{\text{high}}-V_{\text{ex}}^{\text{low}}$ and $A^{\text{high}}-A^{\text{low}}$ are, respectively, the changes in the EV and the ASA upon the destruction, and they are both positive.

For the pressure-induced destruction to occur, $C_2(A^{\text{high}}-A^{\text{low}})$ (negative) must surpass $C_1(V_{\text{ex}}^{\text{high}}-V_{\text{ex}}^{\text{low}})$ (positive) at sufficiently high pressures. In other words, only the structure making the former larger can be stabilized at elevated pressures. The pressure dependence of the structural stability is determined by a subtle balance between these two terms. At low pressures, the structural stability is determined primarily by the EV term [i.e., $C_1(V_{\text{ex}}^{\text{high}}-V_{\text{ex}}^{\text{low}})$] because $|C_2|/C_1\ll 1$. As the pressure becomes higher, both C_1 and $|C_2|$ increase but the increase in the latter is considerably larger, with the result that the ASA term [i.e., $C_2(A_{\text{ex}}^{\text{high}}-A_{\text{ex}}^{\text{low}})$] becomes increasingly more important in determining the structural stability. The transition to the specific structure for which the ASA term prevails over the EV term is induced by applying high pressures. Upon the transition, the ASA is expected to exhibit a remarkable increase while the EV increase is kept sufficiently small.

D. Pressure denaturation of proteins

We consider $-\Delta S/k_{\text{B}}\equiv(-S/k_{\text{B}})^{\text{unfolded}}-\{(-S/k_{\text{B}})^{\text{native}}\}$ where the superscripts "native" and "unfolded" represent the values for the native structure and for an unfolded structure, respectively. $-\Delta S/k_{\text{B}}$ represents the negative of the solvent-entropy change upon the transition from the native structure to the unfolded one. (It should be emphasized that C_3X+C_4Y is fully incorporated in S/k_{B} we calculate.) Figures 3–5 show $-\Delta S/k_{\text{B}}$ upon the structural transition to the random-coil state, nonnative 1, or nonnative 2 for protein G, 1ctf, and 2cro, respectively. The SE of the random-coil state is taken to be the average value calculated for the set of random coils generated for each protein. As the density corresponding to the pressure increases, all the unfolded structures become more destabilized than the native structure in the low-pressure region. This is because C_1 is much larger than $|C_2|$, and in the right-hand side of Eq. (12) the first term dominates, with the result that any structure with larger EV is more destabilized. With a further increase in the pressure, $|C_2|$ grows more rapidly than C_1, making these two coefficients comparable in magnitude in the high-pressure region. Still, for the random-coil state and nonnative 1 the first term is larger than the second term in the right-hand side of Eq. (12) and they continue to increase the relative instability. As a matter of fact, we have tested many more structures than those described in the present paper, but most of them exhibit qualitatively the same behavior. However, several special structures like nonnative 2 display a completely different feature. As the pressure increases further, their relative instability first becomes larger, but beyond a threshold pressure it begins to decrease rather rapidly and they eventually become more stable than the native structure. We have verified that the qualitative aspects of the conclusion are not altered at all when the three-dimensional integral equation theory is employed.

The decomposition into $C_1\Delta V_{\text{ex}}$, $C_2\Delta A$, and $C_3\Delta X+C_4\Delta Y$ in the case of Fig. 3(c) is shown in Fig. 6. The term $C_3\Delta X+C_4\Delta Y$ is much smaller than the other two terms. Thus, the contribution from the curvature term can be ne-

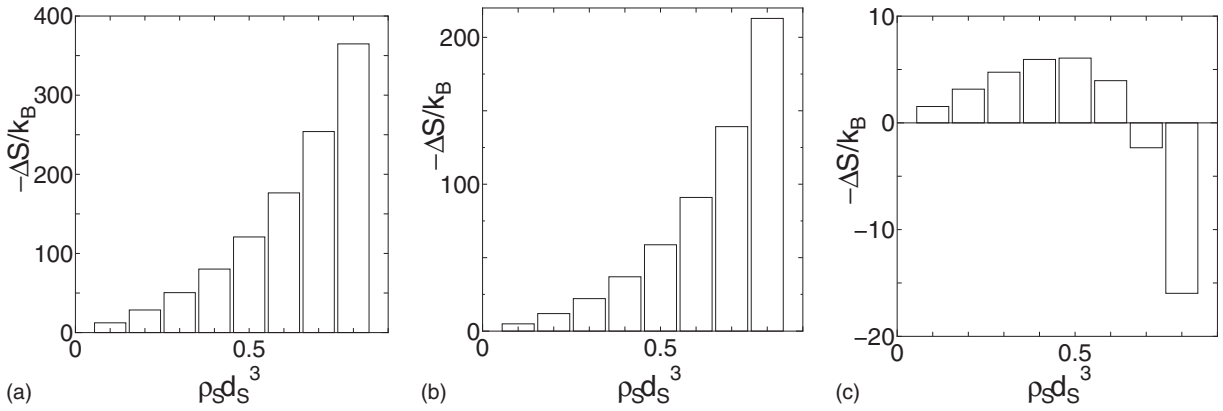

FIG. 3. Negative of the entropy change of solvent scaled by k_B upon the transition from the native structure to (a) the random-coil state, (b) nonnative 1 structure, and (c) nonnative 2 structure of protein G plotted against the bulk solvent density corresponding to the pressure P. $-\Delta S/k_B \equiv (-S/k_B)^{\text{unfolded}} - \{(-S/k_B)^{\text{native}}\}$ where the superscripts "native" and "unfolded" represent the values for the native structure and for the unfolded structure, respectively.

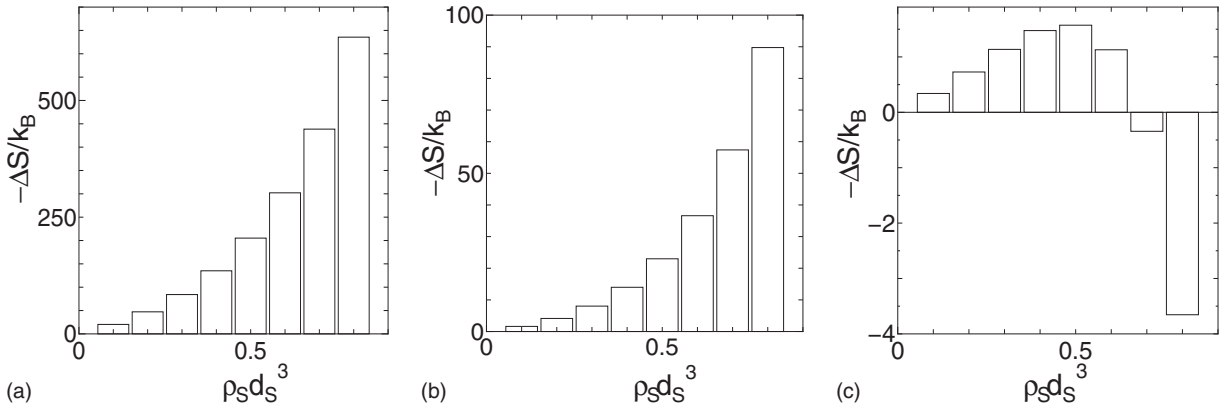

FIG. 4. Negative of the entropy change of solvent scaled by k_B upon the transition from the native structure to (a) the random-coil state, (b) nonnative-1 structure, and (c) nonnative-2 structure of 1ctf plotted against the bulk solvent density corresponding to the pressure P. $-\Delta S/k_B \equiv (-S/k_B)^{\text{unfolded}} - \{(-S/k_B)^{\text{native}}\}$ where the superscripts "native" and "unfolded" represent the values for the native structure and for the unfolded structure, respectively.

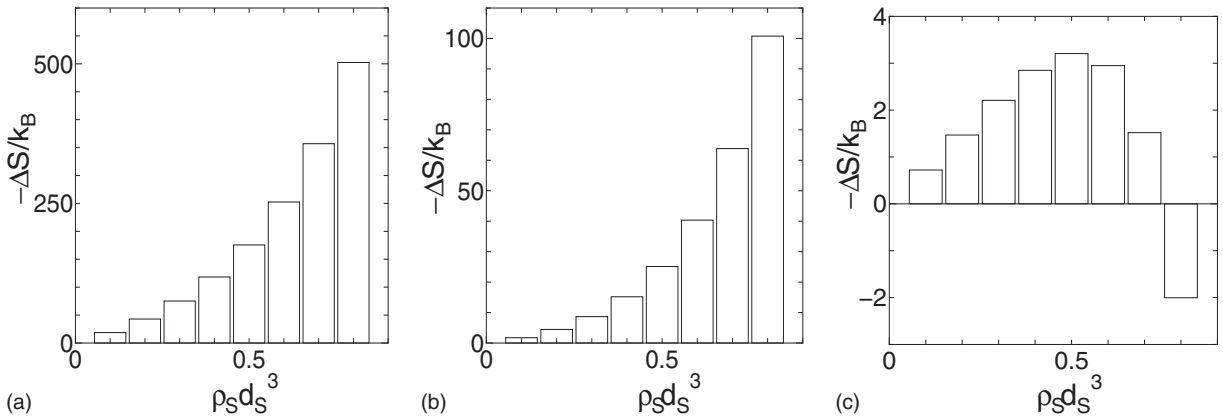

FIG. 5. Negative of the entropy change of solvent scaled by k_B upon the transition from the native structure to (a) the random-coil state, (b) nonnative-1 structure, and (c) nonnative-2 structure of 2cro plotted against the bulk solvent density corresponding to the pressure P. $-\Delta S/k_B \equiv (-S/k_B)^{\text{unfolded}} - \{(-S/k_B)^{\text{native}}\}$ where the superscripts "native" and "unfolded" represent the values for the native structure and for the unfolded structure, respectively.

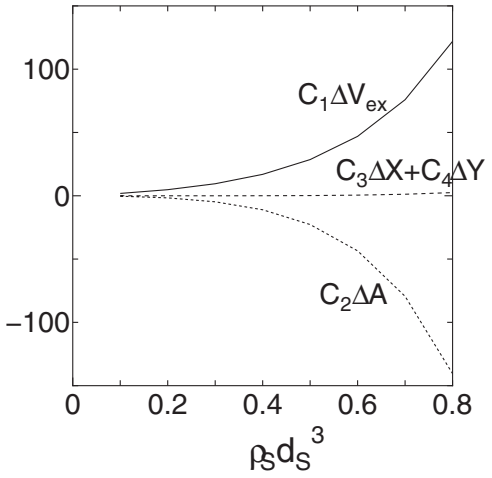

FIG. 6. Decomposition of $-\Delta S$ for nonnative-2 structure of protein G into $C_1\Delta V_{ex}$, $C_2\Delta A$, and $C_3\Delta X+C_4\Delta Y$ at each density.

glected in discussing $-\Delta S/k_B$. The density dependence of $-\Delta S/k_B$ is determined primarily by the EV and ASA terms. In addition, since $C_3\Delta X+C_4\Delta Y$ is positive, pressure denaturation is induced only by the ASA term. We have reached the same conclusion for the other two proteins as well.

Tables I–III give the EV and ASA of the structures considered for protein G, 2cro, and 1ctf, respectively. The values for the random-coil state are those averaged over the 32 or ten random coils generated. The EV follows the order native structure < nonnative 2 < nonnative 1 < random-coil state, and the ASA the order native structure < nonnative 1 < nonnative 2 < random-coil state. Thus, nonnative 2 has a smaller EV and larger ASA. $V_{ex}^{unfold}-V_{ex}^{native}$ and $A^{unfold}-A^{native}$ are small enough and large enough, respectively, to make $|C_2(A^{unfold}-A^{native})|$ larger than $|C_1(V_{ex}^{unfold}-V_{ex}^{native})|$ at sufficiently high pressures. For the random-coil state, $A^{unfold}-A^{native}$ is quite large but $V_{ex}^{unfold}-V_{ex}^{native}$ is too large to invert the relative stability. For structures like nonnative 1, on the other hand, $V_{ex}^{unfold}-V_{ex}^{native}$ is fairly small, but $A^{unfold}-A^{native}$ is not large enough to invert the relative stability. The inversion of the relative stability occurs only for structures whose ASA is considerably larger and whose EV is only moderately larger than in the native structure. These structures can be reached by solvent penetration into the protein interior, causing swelling.

From the standpoint of the morphometric form, pressure denaturation is induced by the negative value of C_2^{multi}, which arises from the protein-solvent-solvent triplet and higher-order correlations. If we considered the SE at the pair correlation level alone, the native structure would be increasingly more stabilized with rising pressure even relative to nonnative 2 because of the positive value of C_2^{pair}, and thus the pressure denaturation could never be elucidated. When solvent particles penetrate into the protein interior or contact the protein surface, the penetration or the contact itself causes an entropic loss. The use of the AO theory, which is based only on C_1^{pair}, would also lead to such a failure.

Here we comment on the previous studies [46] dealing with pressure denaturation of proteins which are concentrated on the partial molar volume (PMV) defined by

$$V_{PMV}=\left(\frac{\partial\mu}{\partial P}\right)_T, \tag{13}$$

where P is the pressure. In those studies the PMV is calculated at low pressures, and structures having smaller PMV than the native structure are identified as denatured ones stabilized at high pressures. However, our results indicate that it is not justified to consider the PMV at low pressures. We first note that (13) can be expressed as

$$V_{PMV}=\left(\frac{\partial\mu}{\partial\rho}\right)_T\left(\frac{\partial\rho}{\partial P}\right)_T. \tag{14}$$

Since $(\partial\rho/\partial P)_T$ is positive, the sign of ΔV_{PMV} can be discussed by looking at $(\partial\Delta\mu/\partial\rho)_T$. From Figs. 3–5, ΔV_{PMV} is positive even for nonnative 2 at low pressures. As the pressure increases ΔV_{PMV} decreases and eventually becomes negative only at sufficiently high pressures. Pressure denaturation should be analyzed by calculating the PMV in the high-pressure region, or, preferably, the solvation free energy or entropy as a function of the pressure.

TABLE I. Excluded volume and solvent-accessible surface area for several structures of protein G. Those of the random-coil state are the average of 32 structures.

	Excluded volume (Å^3)	Solvent-accessible surface area (Å^2)
Native	11600.3	3670.90
Random coil	14002.9	5947.13
Nonnative 1	12326.0	3777.31
Nonnative 2	11926.9	4210.81

TABLE II. Excluded volume and solvent-accessible surface area for several structures of 1ctf. Those of the random-coil state are the average of ten structures.

	Excluded volume (Å^3)	Solvent-accessible surface area (Å^2)
Native	13333.4	4045.62
Random coil	16712.1	7088.28
Nonnative 1	13618.2	4059.55
Nonnative 2	13403.4	4148.24

TABLE III. Excluded volume and solvent-accessible surface area for several structures of 2cro. Those of the random coil structure are the average of ten structures.

	Excluded volume (Å^3)	Solvent-accessible surface area (Å^2)
Native	14794.1	4389.05
Random coil	17536.9	7190.47
Nonnative 1	15101.7	4399.91
Nonnative 2	14950.0	4657.15

E. Comment on the formation-dissociation process of amyloid fibrils

It is experimentally known that the amyloid fibrils are dissociated into monomers when a high pressure is applied to the system [19]. Equation (12) should also be applicable to the formation-dissociation process. "High" and "low" denote monomers and fibrils, respectively. $V_{ex}^{high}-V_{ex}^{low}$ and $A^{high}-A^{low}$ are both positive. According to the experimental results, there are lots of vacant spaces within the fibrils, which water molecules cannot enter [47]. (We emphasize that, even with such small vacant spaces, overlaps of the excluded volumes generated by protein subunits certainly occur, and the EV of the fibrils is smaller than that of the monomers.) Such a feature is in marked contrast to the native structure of a protein in which the backbone and side chains are tightly packed with little space in its interior. Because of the small vacancies, V_{ex}^{low} is significantly large while A^{low} is fairly small. Therefore, upon the dissolution of the amyloid fibrils, $V_{ex}^{high}-V_{ex}^{low}$ can be kept sufficiently small even though $A^{high}-A^{low}$ becomes quite large. The dissolution to monomers whose structures have features like those of nonnative 2 can be the best solution. The monomers cannot be random coils because of the unacceptably large EV increase despite the largest ASA increase. The dissolution of actin filaments with lots of small vacant spaces [20] can be understood in a similar manner. Thus, the folding-unfolding transition of a protein and the formation-dissociation process of amyloid fibrils can be discussed within the same framework, pending theoretical verification in future studies for the latter.

IV. CONCLUSIONS

We have reconsidered a large hard-sphere solute inserted into small hard spheres forming the solvent using the integral equation theory combined with the morphometric approach. The solvent-density profile near the solute and the solvation entropy are calculated for a wide range of bulk solvent densities corresponding to the system pressure. The SE is decomposed into the solute-solvent pair correlation component and the solute-solvent-solvent triplet and higher-order correlation component. Each component is further decomposed into terms that are dependent on the excluded volume generated by the solute, solvent-accessible surface area, and curvature of the accessible surface, respectively.

We have suggested that the attraction between the solute surface and solvent particles is the key point to understand the present result; namely, solvent particles are entropically enriched in the vicinity of the solute. The attraction becomes higher with rising pressure. Although the formation of the enriched layer itself causes an entropic loss, the solvent molecules far outside the solute surface benefit from an even larger entropic gain by the overlap of the EVs generated by the solute and the solvent molecules near the solute surface. Consequently, the solvent entropy of the whole system becomes higher. The attraction originates from the solute-solvent-solvent triplet and higher-order correlations. These results are applied to a complex solute whose structure is changeable using the morphometric approach.

We have then achieved a general framework of pressure effects on the structures formed by the self-assembly of solute molecules driven by solvent entropy. It is experimentally known that a protein is unfolded and the amyloid fibrils are dissociated by applying high pressures. We consider the two different structures stabilized at low and high pressures, respectively. For protein folding and unfolding they are the native structure and an unfolded state, and for amyloid-fibril formation and dissociation they are the fibrils and a set of monomers, respectively. It is argued that the differences between the structures in terms of the EV and ASA play essential roles as indicated in Eq. (12). The structural stability is determined by a subtle balance between the first (positive) and second (negative) terms in the right-hand side of Eq. (12). At low pressures a structure almost minimizing its EV is stabilized, whereas at high pressures a structure with the largest possible ASA together with the EV kept sufficiently small is more favored.

By an analysis of pressure denaturation to illustrate our framework, only a class of special structures is shown to become more stabilized relative to the native structure at sufficiently high pressures. Those structures are characterized by only moderately larger EV and much larger ASA, which is attained by the solvent penetration into the protein interior. The protein-solvent-solvent triplet and higher-order correlations are critical in pressure denaturation. If we consider the protein-solvent pair correlation alone, it is impossible to give an interpretation of pressure denaturation. We have also described how amyloid fibrils are dissociated at high pressures on the basis of the framework, pending theoretical verification in future studies.

In our interpretation, the increase in the free volume occurs for the solvent particles beyond the denser layer formed in the vicinity of the surface. Of course, the solvent particles in the bulk (i.e., those infinitely far from the surface) cannot be influenced and their free volumes remain unchanged. However, the influence reaches a length scale which is much larger than one might expect (i.e., up to positions fairly far from the surface). This can be understood from the following. The solvent particles that are farther from the surface are less influenced, but the number of such solvent particles becomes progressively larger as the distance from the surface increases. In the case of pressure denaturation of a protein, the solvent particles penetrate the protein interior. The gain of larger free volumes should occur for the solvent particles outside the protein and sufficiently far (not infinitely far) from the protein surface.

ACKNOWLEDGMENTS

The development of our computer program for the morphometric approach was made possible by the collaboration with Roland Roth. Also, useful comments from him are greatly appreciated. This work was supported by Grants-in-Aid for Scientific Research on Priority Areas (No. 15076203) from the Ministry of Education, Culture, Sports, Science and Technology of Japan and by the Next Generation Super Computing Project, Nanoscience Program, MEXT, Japan.

APPENDIX: SOLUTE-SOLVENT-SOLVENT TRIPLET AND HIGHER-ORDER CORRELATIONS

We clarify the physical meaning of the solvation entropy at the solute-solvent-solvent triplet and higher-order correlation levels. From Eq. (3), we obtain

$$
\begin{aligned}
-S/k_B &= 4\pi\rho_S \int_0^\infty \left(\frac{1}{2}[h_{US}(r)]^2 \right. \\
&\quad \left. - \frac{1}{2}h_{US}(r)c_{US}(r) - c_{US}(r) \right) r^2 dr \\
&= 4\pi\rho_S \int_0^{d_{US}} \left(\frac{1}{2} - \frac{1}{2}c_{US}(r) \right) r^2 dr \\
&\quad + 4\pi\rho_S \int_{d_{US}}^\infty \left(\frac{1}{2}[h_{US}(r)]^2 \right. \\
&\quad \left. - \frac{1}{2}h_{US}(r)c_{US}(r) - c_{US}(r) \right) r^2 dr \\
&= \frac{\rho_S V_{ex}}{2} - 4\pi\rho_S \int_0^{d_{US}} \left(\frac{1}{2}c_{US}(r) \right) r^2 dr \\
&\quad + 4\pi\rho_S \int_{d_{US}}^\infty \left(\frac{1}{2}[h_{US}(r)]^2 \right. \\
&\quad \left. - \frac{1}{2}h_{US}(r)c_{US}(r) - c_{US}(r) \right) r^2 dr. \qquad \text{(A1)}
\end{aligned}
$$

The relation, $h_{US}(r)=-1$ for $r<d_{US}$, has been used. The excluded volume V_{ex} is $4\pi d_{US}^3/3$. Using Eq. (A1), we can express S^{multi} as

$$
\begin{aligned}
S^{multi}/k_B &= S/k_B - S^{pair}/k_B \\
&= 4\pi\rho_S \int_0^{d_{US}} \left(\frac{1}{2}c_{US}(r) \right) r^2 dr \\
&\quad - 4\pi\rho_S \int_{d_{US}}^\infty \left(\frac{1}{2}[h_{US}(r)]^2 \right. \\
&\quad \left. - \frac{1}{2}h_{US}(r)c_{US}(r) - c_{US}(r) \right) r^2 dr \\
&\quad - 4\pi\rho_S \left(\int_{d_{US}}^\infty [g_{US}(r)-1] r^2 dr \right. \\
&\quad \left. + \int_{d_{US}}^\infty g_{US}(r)\ln[g_{US}(r)] r^2 dr \right) + \frac{\rho_S V_{ex}}{2}. \qquad \text{(A2)}
\end{aligned}
$$

Since $g_{US}(r)=\exp[h_{US}(r)-c_{US}(r)]$ for $r>d_{US}$ in the HNC equation (2) ($b_{\alpha\beta}=0$), we can rearrange Eq. (A2) as follows:

$$
\begin{aligned}
S^{multi}/k_B &= 2\pi\rho_S \int_0^{d_{US}} c_{US}(r) r^2 dr \\
&\quad + 2\pi\rho_S \int_{d_{US}}^\infty [g_{US}(r)-1]\ln[g_{US}(r)] r^2 dr + \frac{\rho_S V_{ex}}{2}.
\end{aligned} \qquad \text{(A3)}
$$

Thus, S^{multi} has an additional term [the first term in the right-hand side of Eq. (A3)] as well as the terms described by $g_{US}(r)$ and V_{ex}. Note that the additional term is not included in S^{pair}. We show hereafter that the solute-solvent-solvent triplet and higher-order correlation levels comes from $c_{US}(r)$.

We first note that the Ornstein-Zernike relation is exact though the HNC closure is approximate [27,48]. From the OZ equation (1a), $c_{US}(r)$ is expressed as

$$
c_{US}(r) = \frac{1}{2\pi^2} \int_0^\infty \frac{H_{US}(k)}{1+\rho_S H_{SS}(k)} \frac{\sin(kr)}{kr} k^2 dk, \qquad \text{(A4)}
$$

where $H_{\alpha\beta}$ is the Fourier transform of $h_{\alpha\beta}(r)$, which is defined by

$$
H_{\alpha\beta} = 4\pi \int_0^\infty h_{\alpha\beta}(r) \frac{\sin(kr)}{kr} r^2 dr. \qquad \text{(A5)}
$$

In the right-hand side of Eq. (A4) we use the following expression:

$$
\begin{aligned}
\frac{H_{US}(k)}{1+\rho_S H_{SS}(k)} &= H_{US}(k) - H_{US}(k)\rho_S H_{SS}(k) + H_{US}(k) \\
&\quad \times [\rho_S H_{SS}(k)]^2 - H_{US}(k)[\rho_S H_{SS}(k)]^3 + \cdots .
\end{aligned} \qquad \text{(A6)}
$$

Here $H_{US}(k)H_{SS}(k)$ in the right-hand side of Eq. (A6) is the Fourier transform of the convolution integral of $h_{US}(r)$ and $h_{SS}(r)$, and the second term represents the solute-solvent-solvent triplet correlation. Likewise, the third and succeeding terms represent the higher-order correlations. Thus, we can conclude that the first term in the right-hand side of of Eq. (A6) contains the effect of the solute-solvent-solvent triplet and higher-order correlation levels through the use of the OZ relation. S^{multi} is not determined only by the effect g_{US} near the solute surface.

We further decompose Eq. (A6) into the following two terms:

$$
\frac{H_{US}(k)}{1+\rho_S H_{SS}(k)} = H_{US}(k) + \Lambda_{US}^{multi}(k), \qquad \text{(A7)}
$$

and define $c_{US}^{multi}(r)$ as

$$
c_{US}^{multi}(r) \equiv \frac{1}{2\pi^2} \int_0^\infty \Lambda_{US}^{multi}(k) \frac{\sin(kr)}{kr} k^2 dk. \qquad \text{(A8)}
$$

From the decomposition (A7), $c_{US}(r)$ is represented as

$$
c_{US}(r) = h_{US}(r) + c_{US}^{multi}(r). \qquad \text{(A9)}
$$

Using Eq. (A9) and $h_{US}(r)=-1$ at $r<d_{US}$, S^{multi} becomes

$$
\begin{aligned}
S^{multi} &= 2\pi\rho_S \int_0^{d_{US}} [h_{US}(r) + c_{US}^{multi}(r)] r^2 dr \\
&\quad + 2\pi\rho_S \int_{d_{US}}^\infty [g_{US}(r)-1]\ln[g_{US}(r)] r^2 dr + \frac{\rho_S V_{ex}}{2} \\
&= 2\pi\rho_S \int_0^{d_{US}} c_{US}^{multi}(r) r^2 dr
\end{aligned}
$$

$$+2\pi\rho_S\int_{d_{US}}^{\infty}[g_{US}(r)-1]\ln[g_{US}(r)]r^2dr. \quad \text{(A10)}$$

Since $g_{US}(r)$ does not significantly deviate from 1 for $r > d_{US}$, both $g_{US}(r)-1$ and $\ln[g_{US}(r)]$ are very small. In the right-hand side of Eq. (A10), the second term is much smaller than the first one and considerably smaller than S_A^{pair}/k_B. The effect of the solute-solvent-solvent triplet and higher-order correlations forms a major part of S^{multi}. Thus, the solvation entropy has been decomposed into the pair correlation component and the triplet and higher-order correlation component almost completely.

[1] M. Kinoshita, J. Chem. Phys. **116**, 3493 (2002).
[2] M. Kinoshita, Chem. Phys. Lett. **387**, 54 (2004).
[3] Y. Harano and M. Kinoshita, Chem. Phys. Lett. **399**, 342 (2004).
[4] Y. Harano and M. Kinoshita, Biophys. J. **89**, 2701 (2005).
[5] M. Kinoshita, Chem. Eng. Sci. **61**, 2150 (2006).
[6] R. Roth, Y. Harano, and M. Kinoshita, Phys. Rev. Lett. **97**, 078101 (2006).
[7] Y. Harano, R. Roth, and M. Kinoshita, Chem. Phys. Lett. **432**, 275 (2006).
[8] Y. Harano, R. Roth, Y. Sugita, M. Ikeguchi, and M. Kinoshita, Chem. Phys. Lett. **437**, 112 (2007).
[9] T. Yoshidome, M. Kinoshita, S. Hirota, N. Baden, and M. Terazima, J. Chem. Phys. **128**, 225104 (2008).
[10] N. Baden, S. Hirota, T. Takabe, N. Funasaki, and M. Terazima, J. Chem. Phys. **127**, 175103 (2007).
[11] H. Ohtaka, A. Schon, and E. Freire, Biochemistry **42**, 13659 (2003).
[12] J. Kardos, K. Yamamoto, K. Hasegawa, H. Naiki, and Y. Goto, J. Biol. Chem. **279**, 55308 (2004).
[13] C. F. Bonafe, C. M. Vital, R. C. Telles, M. C. Goncalves, M. S. Matsuura, F. B. Pessine, D. R. Freitas, and J. Vega, Biochemistry **37**, 11097 (1998).
[14] M. Kasai, S. Asakura, and F. Oosawa, Biochim. Biophys. Acta **57**, 13 (1962).
[15] R. R. Swezey and G. N. Somero, Biochemistry **21**, 4496 (1982).
[16] B. Lee and F. M. Richards, J. Mol. Biol. **55**, 379 (1971).
[17] C. Clery, F. Renault, and P. Masson, FEBS Lett. **370**, 212 (1995).
[18] F. Meersman, C. M. Dobson, and K. Heremans, Chem. Soc. Rev. **35**, 908 (2006).
[19] D. Foguel *et al.*, Proc. Natl. Acad. Sci. U.S.A. **100**, 9831 (2003).
[20] T. Ikkai and T. Ooi, Biochemistry **5**, 1551 (1966).
[21] P. S. Niranjan, P. B. Yim, J. G. Forbes, S. C. Greer, J. Dudowicz, K. F. Freed, and J. F. Douglas, J. Chem. Phys. **119**, 4070 (2003).
[22] Y. Harano and M. Kinoshita, J. Phys.: Condens. Matter **18**, L107 (2006).
[23] Y. Harano and M. Kinoshita, J. Chem. Phys. **125**, 024910 (2006).
[24] S. Asakura and F. Oosawa, J. Chem. Phys. **22**, 1255 (1954).
[25] S. Asakura and F. Oosawa, J. Polym. Sci. **33**, 183 (1958).
[26] P. M. König, R. Roth, and K. R. Mecke, Phys. Rev. Lett. **93**, 160601 (2004).
[27] J. P. Hansen and L. R. Mcdonald, *Theory of Simple Liquids* (Academic Press, London, 1986).
[28] M. Kinoshita and M. Harada, Mol. Phys. **65**, 599 (1988).
[29] M. Kinoshita, S. Iba, K. Kuwamoto, and M. Harada, J. Chem. Phys. **105**, 7177 (1996).
[30] M. Kinoshita, S. Iba, K. Kuwamoto, and M. Harada, J. Chem. Phys. **105**, 7184 (1996).
[31] T. Morita, Prog. Theor. Phys. **23**, 829 (1960).
[32] T. Morita and K. Hiroike, Prog. Theor. Phys. **25**, 537 (1961).
[33] H. S. Ashbaugh and M. E. Paulaitis, J. Phys. Chem. **100**, 1900 (1996).
[34] M. Kinoshita, N. Matubayasi, Y. Harano, and M. Nakahara, J. Chem. Phys. **124**, 024512 (2006).
[35] M. Kinoshita, J. Chem. Phys. **128**, 024507 (2008).
[36] B. Park and M. Levitt, J. Mol. Biol. **258**, 367 (1996).
[37] T. Imai, Y. Harano, M. Kinoshita, A. Kovalenko, and F. Hirata, J. Chem. Phys. **126**, 225102 (2007).
[38] Y. Harano, T. Yoshidome, and M. Kinoshita, J. Chem. Phys. **129**, 145103 (2008).
[39] We note that the morphometric approach is mathematically rigorous as long as the systems satisfy the three conditions required by the Hadwiger theorem [40]: motion invariance, continuity, and additivity [26,41]. The morphometric approach is inappropriate for fluids near the critical point in the phase diagram because the additivity and continuity conditions are broken [26,41] due to the long correlation length of the solvent. However, using the solvent-solvent total correlation function $h_{SS}(r)$ at the highest solvent density ($\rho_S d_S^3=0.8$), we have confirmed that the correlation decays quite rapidly: $|h_{SS}(r)| < 10^{-2}$ for $r > 5d_S$. (The same behavior is observed for the solute-solvent total correlation function.) Thus, the correlation is shorter ranged than the size of the protein in any structure tested (even for the native structure that is the most compact, the size is approximately $10d_S$). Therefore, the additivity and continuity conditions are satisfied and the morphometric approach is valid for the present system.
[40] H. Hadwiger, *Vorlesungen über Inhalt, Oberfläche und Isoperimetrie* (Springer, Berlin, 1957).
[41] H. Hansen-Goos, R. Roth, K. Mecke, and S. Dietrich, Phys. Rev. Lett. **99**, 128101 (2007).
[42] M. L. Connolly, J. Appl. Crystallogr. **16**, 548 (1983).
[43] M. L. Connolly, J. Am. Chem. Soc. **107**, 1118 (1985).
[44] M. Ikeguchi and J. Doi, J. Chem. Phys. **103**, 5011 (1995).
[45] M. Kinoshita, Chem. Phys. Lett. **387**, 47 (2004).
[46] T. Imai, S. Ohyama, A. Kovalenko, and F. Hirata, Protein Sci. **16**, 1927 (2007).
[47] K. Akasaka, A. R. Abdul Latif, A. Nakamura, K. Matsuo, H. Tachibana, and K. Gekko, Biochemistry **46**, 10444 (2007).
[48] P. Attard and G. N. Patey, J. Chem. Phys. **92**, 4970 (1990).